

# Observation-based dissipation and input terms for WAVEWATCH III™: implementation and simple simulations

Stefan Zieger\*<sup>‡</sup>, Alexander V. Babanin\*, W. Erick Rogers<sup>†</sup> and Ian R. Young<sup>§</sup>

\* *Swinburne University of Technology, Melbourne, Victoria, Australia*

<sup>†</sup> *Naval Research Laboratory, Stennis Space Center, Mississippi*

<sup>§</sup> *Australian National University, Canberra, A.C.T., Australia*

## Abstract

Observational data collected at Lake George, Australia resulted in new insights on the processes of wind wave interaction and white-capping dissipation and consequently new parameterisations of these source terms. The new wind input source term (Donelan et al., 2006; Babanin et al., 2007a) accounts for the dependence of growth increment on wave steepness, and on airflow separation with relative reduction of the growth under extreme wind conditions. The new white-capping dissipation source term (Babanin and Young, 2005; Young and Babanin, 2006) consists of two terms, the inherent breaking term and dissipation induced by longer waves. The present implementation follows Rogers et al. (submitted). Two novel parameterisations are validated against existing source terms and buoy measurements for windsea-dominated conditions in duration-limited simulations and hindcast.

## 1 Introduction

Numerical simulation of the evolution of wind-wave energy density spectrum is routinely conducted in wave forecast and hindcast. In third-generation (3G) models, wind-wave evolution is described by the wave energy balance equation (1) which totals all energy fluxes, source terms  $S_{tot}$ , represented by all physical processes that contribute to wind-wave evolution. The wave energy balance equation can be written as (Young, 1999):

$$\frac{\partial F}{\partial t} + \nabla \cdot c_g F = S_{tot}. \quad (1)$$

The first term of the left hand side of (1) represents the rate of net change of wave spectral energy  $F = F(\omega, \theta, t, \mathbf{x})$ , a function of frequency  $\omega = 2\pi f$ , direction  $\theta$ , time  $t$  and space  $\mathbf{x}$ . The second term represents the advection of wave energy at group velocity  $c_g$ . It is generally accepted (e.g., Komen et al., 1994; Young, 1999; Tolman, 2009) that for deep water, the total source term (2) that contributes to wind-wave evolution is based on three physical processes, all of which are spectral functions  $S(\omega, \theta)$ . These processes are atmospheric input  $S_{in}$ , wave dissipation  $S_{ds}$ , and nonlinear interactions between wave components of different frequencies  $S_{nl}$ :

$$S_{tot} = S_{in} + S_{ds} + S_{nl} \quad (2)$$

Babanin and Westhuysen (2008), and Babanin (2011) argued that these individual terms have to be further subdivided. For example,  $S_{ds}$  is a sum of inherent and cumulative wave-breaking dissipation, of dissipation due to interaction with

turbulence in the water and the air, with the adverse wind and so on. Provision should be made to let individual dissipation mechanism ease and still let swell dissipation continue. In transitional water and water of finite depth additional processes, for example wave-bottom interactions and depth-induced breaking, become significant in (2) and have to be considered in the total source term  $S_{tot}$  (Tolman, 2009). This paper only focusses on wind input  $S_{in}$  and dissipation  $S_{ds}$ . Third-generation wave models such as WAVEWATCH III™, use the wave action spectrum  $N$  directly to calculate the source terms. The wave action spectrum is a wavenumber-direction spectrum  $N(k, \theta)$  which can be converted to the wave energy spectrum using Jacobian transformation:  $F(\omega, \theta) = N(k, \theta)\omega/c_g$  (Tolman, 2009). The observation-based source terms are given in form of the more traditional frequency-direction spectrum for wind input and dissipation hereafter. The present version of WAVEWATCH III™ (3.14) features three source term packages: WAM3 physics (Komen et al., 1984), WAM4 physics (Ardhuin et al., 2010), and Tolman and Chalikov (1996) physics.

The objective here is to test observation-based source terms as implemented in WAVEWATCH III™ for wind-dominated conditions in duration-limited simulations and hindcast. The paper is structured as follows: Section 2 outlines novel features of the observation-based source terms including the source functions; section 3 describes the model setup used in both simulations. The duration-limited simulation is a purely academic test while the hindcast is based on the Naval Research Laboratory (NRL) test bed for Lake Michigan. Results obtained from those two simulations are shown in subsections. Section 4 provides a summary and directions for future work.

---

<sup>‡</sup> *Corresponding author address: szieger@swin.edu.au*  
Proc. of the 12th Int. Workshop on Wave Hindcasting and Forecasting, 30 October – 4 November 2011, Kohala Coast, HI

## 2 Observation-based source terms

Spectral parametrisations of wind input and wave dissipation are based on field experiments carried out during the Australian Shallow Water Experiment (AUSWEX) at Lake George, New South Wales, Australia. For the wind input, the boundary layer study is described in detail by Donelan et al. (2005) which was later parameterised by Donelan et al. (2006) as spectral functions to be used in wave models. For wave breaking and dissipation, field data unveiled novel features of the wave breaking process (Banner et al., 2000; Babanin et al., 2001) and spectral dissipation (Babanin and Young, 2005; Young and Babanin, 2006).

So far, the new source terms have been implemented and calibrated for two 3G wave models: (1) the one-dimensional research model WAVETIME<sup>1</sup> (Tsagareli et al., 2010) and (2) the U.S. Navy operational forecast model SWAN<sup>2</sup> (Rogers et al., submitted). Wind input and dissipation functions described in section 2 follow the implementation of the NRL operational model as proposed by Rogers et al. (submitted).

In order to demonstrate calculations with new source terms for wind input  $S_{in}$  and wave dissipation  $S_{ds}$  a “transitional spectrum” is used following a parametric Pierson-Moskowitz spectrum used by Tsagareli et al. (2010) and Babanin et al. (2010). The “transitional spectrum” (3) features the transition from  $\omega^{-4}$  slope to  $\omega^{-5}$  at the transition frequency. Here, a transition frequency of  $3\omega_{PM}$  was selected where  $\omega_{PM}$  ( $= 2\pi \cdot 0.13g/U_{10}$ ) refers to the peak frequency of the Pierson-Moskowitz spectrum for a given wind speed 10 m above the surface  $U_{10}$  (see Pierson and Moskowitz, 1964).

$$F(\omega) = \begin{cases} \frac{\alpha g^2}{\omega^4 \omega_p} \exp(-[\omega_{PM}/\omega]^4) & \text{for } \omega \leq 3\omega_{PM} \\ F(3\omega_{PM}) [(3\omega_{PM})/\omega]^5 & \text{for } \omega > 3\omega_{PM} \end{cases} \quad (3)$$

The “transitional spectrum” is given in (3), where  $\alpha = 0.0054$  is the Philips constant for the Pierson-Moskowitz spectrum,  $\omega_p$  represents the peak frequency, and  $g$  is the gravitational acceleration. An example of the “transitional spectrum” for wind speed of  $U_{10} = 8 \text{ ms}^{-1}$  is shown in the top panel of Figure 1 where the transition from  $\omega^{-4}$  slope to  $\omega^{-5}$  is marked with the bold dotted line.

### 2.1 Wind input

The wind input function represents the energy flux transferred from wind to waves. It is widely accepted

that wind-wave development is due to wave-induced pressure acting on the slopes of the waves (Donelan et al., 2006). AUSWEX data analysis and the wind input parameterisation reported by Donelan et al. (2006) dependencies that have not been reported in previous experiments.

Measurements of wave growth were available for a range of wind-forcing conditions including very young waves  $U_{10}/c_p = 5.1 - 7.6$  ( $c_p$  is the phase speed at the spectral peak) of varying steepness. This unique dataset unveiled a few novel features: (i) full air-flow separation with relative reduction for strong winds, (ii) non-linear relationship between phase speed, crest curvature and the slope of the waves, and (iii) the dependence of wave growth on wave steepness (Donelan et al., 2006; Babanin et al., 2007a). The resulting parameterisation of the wind input affects the momentum flux parameterisation in opposing ways; enhancement for moderate winds and reduction for strong wind forcing.

#### 2.1.1 Novel features

Full air-flow separation means that the wind detaches from the flow essentially skipping the wave troughs before it re-attaches on the windward side of the wave crest. Compared to the non-separated flow, the imposed wind input pressure is relatively weaker under full air-flow separation (Donelan et al., 2006). Full air-flow separation was also part of laboratory experiments conducted by Reul et al. (1999).

The wind input  $S_{in} = \gamma\omega F$  is a function of the wave energy spectrum  $F$  and the growth rate of the wind-waves  $\gamma$ , hence it is linear dependent (Komen et al., 1984). In terms of friction velocity  $u_*$ , for example, the relative growth rate  $\gamma/\omega$  is a function of the ratio of wind speed over phase speed. Empirical fitting of the growth rate typically follows the form  $\gamma/\omega = \rho_{\frac{a}{w}} \beta (u_*/c)^n$ , where  $\rho_{\frac{a}{w}}$  is the ratio of densities of air and water,  $\beta$  is a non-dimensional constant, and  $n$  is an exponent of either  $n = 1$  as in WAM3 or  $n = 2$  as in WAM4 (Komen et al., 1984; Tolman, 2009).

AUSWEX field data also revealed that the wind-wave growth rate  $\gamma$  depends on wave steepness  $ak$  ( $a$  being the wave amplitude), which has previously been considered as unrelated in potential theory for gravity waves. Donelan et al. (2006) showed that wave steepness is connected to the phase shift and the normalised induced pressure amplitude, and that potential flow is only valid as  $ak \rightarrow 0$ . In the final parameterisation the wave steepness  $ak$  is replaced by the spectral saturation  $B_n$  (Phillips, 1984). Thus, the growth rate  $\gamma$  obtained from the Lake George data

<sup>1</sup> developed by G. van Vledder (van Vledder, 2002)

<sup>2</sup> “Simulating WAVes Nearshore” (Booij et al., 1999)

is also a function of the wave action spectrum, which in turn makes the wind input non-linear dependent on the action spectrum.

### 2.1.2 Implementation

The parameterisation of the wind input  $S_{in}$  as proposed by Donelan et al. (2006) is designed to work from young wind-waves to mature seas, i.e. for conditions of light, moderate, and strong wind forcing. The observation-based wind input  $S_{in}$  was estimated from the quadrature spectrum based on measurements of elevation and pressure at the sea surface (Donelan et al., 2006). The proposed wind input is given in (4)–(8) (Donelan et al., 2006; Tsagareli et al., 2010; Rogers et al., submitted).

$$S_{in}(\omega, \theta) = \rho_{\frac{a}{w}} \omega \gamma(\omega, \theta) F(\omega, \theta) \quad (4)$$

$$\gamma(\omega, \theta) = G \sqrt{B_n} W \quad (5)$$

$$G = 2.8 - [1 + \tanh(10\sqrt{B_n}W - 11)] \quad (6)$$

$$B_n = A(\omega) F(\omega) k^3 c_g \quad (7)$$

$$W = (U_{10}/c - 1)^2 \quad (8)$$

Donelan et al. (2006) calibrated the growth rate (5) based on winds 10 m above mean surface  $U_{10}$ . However, 3G wave models typically scale growth rate with friction velocity  $u_*$  and therefore a scaling of  $C_d = (U_{10}/u_*)^2$  was selected in Rogers et al., where  $C_d$  is the drag coefficient given in (13). The value for the drag coefficient depends on various physical parameters and the scatter of experimental data is usually large (for a review see Babanin and Makin, 2008). Nevertheless, the flux computation is typically parameterised as a function of wind speed and is customisable in WAVEWATCH III™. The directional distribution of (8) is implemented as in (9) with  $c$  being the phase speed:

$$W(\omega, \theta) = \max\left\{0, \frac{\sqrt{C_d} u_*}{c} \cos(\theta - \theta_w) - 1\right\}^2. \quad (9)$$

Spectral separation (7), as a measure of wave steepness, is a function of wave energy density  $F(\omega)$  and narrowness  $A(\omega)$  of the directional distribution at a frequency (Babanin and Soloviev, 1998b) in which  $F(\omega) = \int F(\omega, \theta) d\theta$  being the non-directional energy density spectrum. The directional narrowness (10) is inversely given by integration of the normalised energy density spectrum over all directions, where the normalisation is based on the maximum value in the dominant wave direction  $\mathbf{F}(\omega) = \max\{F(\omega, \theta)\}$ , for all directions  $\theta \in [0, 2\pi]$  (Babanin and Soloviev, 1998b).

$$\frac{1}{A(\omega)} = \int_0^{2\pi} \frac{F(\omega, \theta)}{\mathbf{F}(\omega)} d\theta \quad (10)$$

Note that the spectral saturation  $B_n$  is then non-directional and was applied to all directions in order to calculate the directional growth rate  $\gamma(\omega, \theta)$ .

### 2.1.3 Wind stress

The exchange of momentum between the wind, the atmosphere, and the water is determined by the wind stress, a form of action exerted by the wind on the surface and is an indicator of the strength of air-sea interaction (Tsagareli et al., 2010). Close to the surface, the contribution to the total stress  $\tau$  is due to wave-induced stress  $\tau_w$ , turbulent stress  $\tau_t$ , and viscous stress  $\tau_v$ . At the surface, the turbulent momentum flux in the boundary layer approaches zero and therefore turbulence vanishes (Tsagareli et al., 2010). As a result, the total stress at the surface can be written as:

$$\tau = \tau_v + \tau_w \quad (11)$$

Calculation of the wave-induced stress requires knowledge on the drag coefficient  $C_d$  and the viscous drag coefficient  $C_v$  in order to calculate  $\tau$  and  $\tau_v$ , respectively. The drag coefficient is used to translate winds in the boundary layer to the wind stress at the surface. Let  $\rho_a$  be the density of the air then the total stress can be computed with  $\tau = \rho_a C_d U_{10}^2 = \rho_a u_*^2$  and the viscous stress with  $\tau_v = \rho_a C_v U_{10}^2$ . Substituting both expressions into (11) yields the value for the wave-induced stress:

$$\tau_w = \rho_a U_{10}^2 (C_d - C_v). \quad (12)$$

For the drag coefficient, parameterisation (13) was selected as proposed by Hwang (2010) which accounts for saturation, and even decline for extreme winds, of the sea drag at wind speeds in excess of  $30 \text{ m s}^{-1}$ . To prevent  $u_*$  from dropping to zero at very strong winds  $U_{10} \geq 50.33 \text{ m s}^{-1}$ , expression (13) was modified to yield  $u_* = 2.026 \text{ m s}^{-1}$  (Rogers et al., submitted).

$$C_d \times 10^5 = 80.58 + 9.67U_{10} - 0.16U_{10}^2 \quad (13)$$

The viscous drag coefficient was parameterised as a function of wind speed from data by Banner and Peirson (1998):

$$C_v \times 10^3 = 1.1 - 0.05U_{10}. \quad (14)$$

The wave-induced stress (12) is used as a principal constraint for the wind input. The constraint is that the normal stress  $\tau_n$  obtained from integration over the wind-momentum-input function should be equal to wave-induced stress:  $\tau_n = \tau_w$ . Let  $\rho_w$  be the density of water and  $S_{in}(\omega)$  be the non-directional form of the wind input in radian frequency space:  $S_{in}(\omega) = \int_0^{2\pi} S_{in}(\omega, \theta) d\theta$ , then the normal stress  $\tau_n$  can be calculated from the wind-momentum-input:

$$\tau_n = \rho_w g \int_{\omega_0}^{\omega_1} \frac{S_{in}(\omega)}{c(\omega)} d\omega. \quad (15)$$

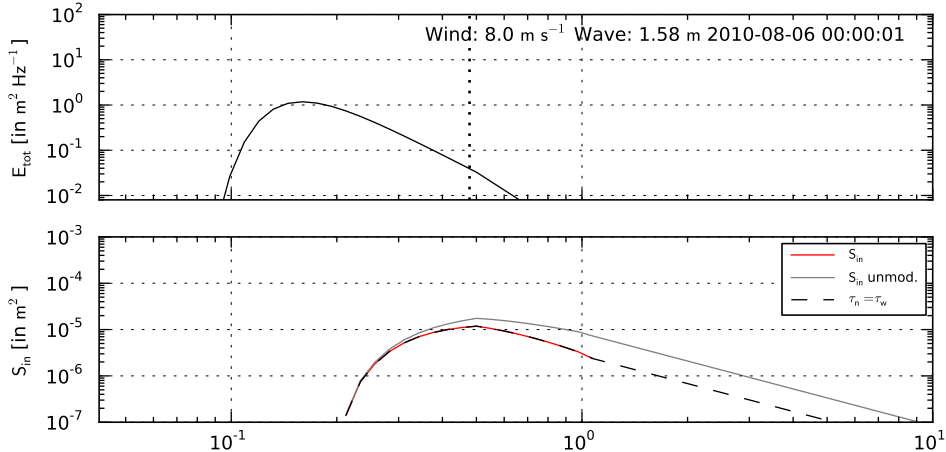


Fig. 1: Wind source term computation on (top panel) “transitional spectrum” (3) for wind speed of  $8 \text{ m s}^{-1}$  with transition from  $f^{-4}$  to  $f^{-5}$  at  $f = 0.48 \text{ Hz}$  (dotted line). The lower panel shows the non-directional wind input (4) based on the prescribed spectrum with (red solid line) and without (gray solid line) reduction (16) applied to match the constraint for the wind input. The highest discrete frequency of the spectrum is  $f = 1.07 \text{ Hz}$  with extrapolation up to  $10 \text{ Hz}$  shown (grey solid and black dashed lines).

Integral limits in (15) range from the first discrete frequency of the spectrum  $\omega_0$  up to the high frequency tail  $\omega_1 = 20\pi$  (i.e.  $10 \text{ Hz}$ ). If the highest discrete frequency of the spectrum is less than  $\omega_1$ , a diagnostic tail up to  $20\pi$  is attached to the wind input using an approximation for the spectral slope:  $S_{in}(\omega) \propto \omega^{-2}$ . Note that, for  $F(\omega) \propto \omega^{-5}$  the Donelan et al. (2006) wind input has exactly that slope at the highest discrete frequency of the spectrum. In order to satisfy the constraint and in case of  $\tau_n > \tau_w$ , a frequency dependent factor  $L$  (16) is applied to reduce energy from the high frequency part of the spectrum:  $S_{in}(\omega) = L(\omega) S_{in}(\omega)$ :

$$L(\omega) = \min\left\{1, \exp(\mu [1 - U_{10}/c])\right\}. \quad (16)$$

The reduction (16) follows an exponential form designed to disproportionately reduce energy from the discrete part of the spectrum. The strength of reduction is controlled by parameter

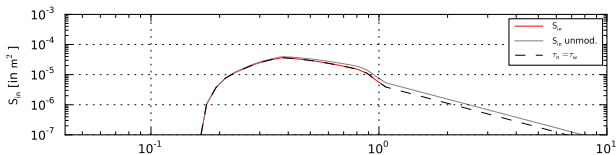


Fig. 2: Same as Fig. 1 but for “transitional spectrum” with  $U_{10} = 10 \text{ m s}^{-1}$ .

$\mu$  where greater energy is reduced at high frequencies with only little impact on the energy-dominant part of the spectrum, where the wind input was actually measured by Donelan et al. (2006). The value of  $\mu$  is dynamically calculated by iteration at each integration time step.

An illustrative example for the implemented wind input source term is given in Figure 2 where the wind input is shown as a function of frequency  $f$  based on (Fig. 1) the “transitional spectrum” (3) for a wind speed of  $8 \text{ m s}^{-1}$ . Also shown is the disproportional reduction in energy of the spectrum to match the imposed constraint on the wind stress. In order to calculate the normal stress (15) the wind input spectrum was extrapolated to  $\omega_1 = 20\pi$ . Note, that the disproportional reduction of energy only applies to the discrete part of the spectrum with a constant reduction of energy in the diagnostic tail to maintain the spectral slope of the tail. A substantial part of the reduction of energy occurs at the higher frequencies of the discrete spectrum and in the diagnostic tail, however, as illustrated in Figure 2, such reduction is less significant when the wind exceeds  $10 \text{ m s}^{-1}$  partially due to air-flow separation, with relative reduction of energy for strong winds.

## 2.2 Wave dissipation

Wave dissipation  $S_{ds}$  in this paper is attributed to energy loss due to wave breaking and is implemented as a negative contribution of energy in the total source term equation (2) in WAVEWATCH III<sup>TM</sup> (Tolman, 2009). Wave breaking and dissipation has been poorly understood and served in operational wave models as tuning parameterisation to outbalance residual energy of the wind input, but lately observations and numerical modelling made understanding of this process available for parameterisations based on physics of the phenomenon (Babanin, 2011).

### 2.2.1 Novel features

AUSWEX data analysis yield three novel features of processes of wave breaking and spectral dissipation namely: (i) the threshold behaviour of wave breaking (initially observed by Banner et al., 2002; Babanin et al., 2001), (ii) the cumulative dissipative effect due to breaking and dissipation of short waves affected by longer waves (Babanin et al., 2010), and (iii) direct dependence of the dissipation on the wind input when the wind forcing is very strong (Babanin, 2011). The threshold behaviour postulates that waves will not break unless they exceed a generic steepness in which case the wave breaking probability depends on the level of exceedence above the threshold (Babanin et al., 2010). For spectral wave models, Babanin and Young (2005), Young and Babanin (2006) and Babanin et al. (2007b) suggested quantitative formulations of the new dissipation term that accommodate threshold behaviour. The cumulative dissipation effect is a previously known physical feature (e.g. Phillips, 1961; Longuet-Higgins and Stewart, 1961), but until recently was not accounted for in the dissipation term of spectral wave models. Therefore, the wave dissipation term  $S_{ds}$  consists of two distinct terms (“two-phase” behaviour): an inherent breaking component  $T_1$  and forced dissipation term  $T_2$  (Babanin et al., 2010; Rogers et al., submitted). The third feature is important at the spectrum tail or at very strong wind forcing. It signifies a condition when the wind input is so strong that the nonlinear interactions are not able to transfer exclusive energy flux, and it is dissipated locally through excessive breaking.

### 2.2.2 Implementation

The “two-phase” behaviour of the wave breaking and dissipation term is implemented as:

$$S_{ds}(\omega, \theta) = (T_1 + T_2) F(\omega, \theta), \quad (17)$$

where  $T_1$  is the inherent breaking term and  $T_2$  accounts for the cumulative effect of short-wave breaking due to longer waves. The threshold spectral density  $F_T$  is calculated as in (18), where  $k$  is the wavenumber and with  $\varepsilon_T = 0.035^2$  being the empirical constant for the wave breaking probability (Babanin et al., 2007b):

$$F_T(\omega) = \frac{\varepsilon_T}{A(\omega) c_g k^3}. \quad (18)$$

Furthermore, let the level of exceedence above the critical threshold spectral density at which stage wave breaking is prominent being defined as  $\Delta(\omega) = F(\omega) - F_T(\omega)$ , and  $\mathcal{F}(\omega)$  being a generic spectral density (see later this section), then the inherent breaking component can be calculated as:

$$T_1(\omega) = a_1 A(\omega) \frac{\omega}{2\pi} \left[ \frac{\Delta(\omega)}{\mathcal{F}(\omega)} \right]^L. \quad (19)$$

The cumulative dissipation term, is not local in frequency space and is based on an integral that grows towards higher frequencies dominating at smaller scales:

$$T_2(\omega) = a_2 \int_0^\omega A(w) \left[ \frac{\Delta(w)}{\mathcal{F}(w)} \right]^M dw. \quad (20)$$

Since the cumulative term (20) is based on integration with altering cut-off frequency, it will not destabilize longer waves and force them to break (Babanin et al., 2010; Rogers et al., submitted).

The dissipation terms (19) and (20) depend on five selected parameters: a generic spectral density  $\mathcal{F}(\omega)$  used for normalisation, and four coefficients  $a_1$ ,  $a_2$ ,  $L$ , and  $M$ . In previous studies, Babanin et al. (2010) and Tsagareli et al. (2010) selected the spectral density  $F(\omega)$  as generic spectrum for normalisation, whereas Ardhuin et al. (2010) selected the threshold spectral density  $F_T(\omega)$ . The coefficients  $L$  and  $M$  control the strength of the normalised threshold spectral density  $\Delta(\omega)/\mathcal{F}(\omega)$  of the dissipation terms. Rogers et al. (submitted) recently calibrated the dissipation terms based on duration-limited academic tests and proposed four sets of coefficients listed in Table 1. Banner et al. (2002) introduced the directional narrowness  $A(\omega)$  as correction for the directional spread to reconcile observed values of the wave-breaking threshold across different bands. Proceeding studies by Babanin et al. (2007b) and Babanin (2009) showed that such correction does not affect the magnitude of the threshold value used in the dissipation terms. Consequently, the directional narrowness parameter is set to unity  $A(\omega) \approx 1$  in all calculations.

Tab. 1: Generic spectral density  $\mathcal{F}(\omega)$  used for normalisation, and four coefficients for wave dissipation terms (19) and (20) after Rogers et al. (submitted).

	<b>F(ω)</b>	<b>L</b>	<b>M</b>	<b>a<sub>1</sub></b>	<b>a<sub>2</sub></b>
DL1M1	F	1	1	2.0 10 <sup>-4</sup>	1.6 10 <sup>-3</sup>
UL2M2	F <sub>T</sub>	2	2	8.8 10 <sup>-6</sup>	1.1 10 <sup>-4</sup>
UL1M4	F <sub>T</sub>	1	4	5.7 10 <sup>-5</sup>	3.2 10 <sup>-6</sup>
UL4M4	F <sub>T</sub>	4	4	5.7 10 <sup>-7</sup>	8.0 10 <sup>-6</sup>

Based on the “transitional spectrum” described earlier, Figure 3 gives an illustrative example for two of the models which shows first-order dependence (DL1M1) and fourth-order dependence (UL4M4) of the dissipation terms. With higher-order, the majority of dissipated energy shifts from lower frequencies towards higher frequencies in the spectrum. Figure 3 also shows the relative contribution of the inherent breaking term  $T_1$  and the cumulative dissipation term  $T_2$ . This is consistent with observations from the real ocean

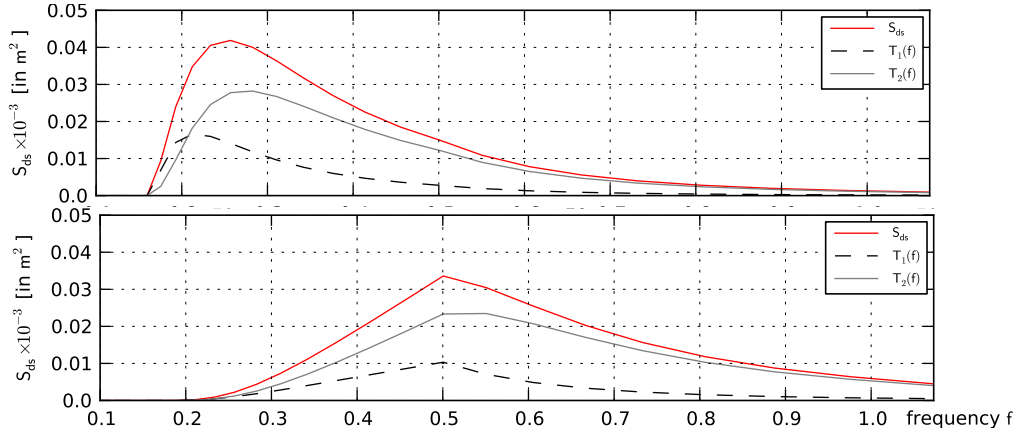


Fig. 3: Dissipation source term computation on “transitional spectrum” (Fig. 1 top panel) for wind speed of  $8 \text{ m s}^{-1}$ . Source terms  $S_{ds} = T_1 + T_2$  are shown as a function of frequency  $f$  for coefficients (top) DL1M1 and (bottom) UL4M4 (see Tab. 1).

in which for fully developed waves the dissipation is dominated by the cumulative wave breaking  $T_2$  (Babanin et al., 2010). Hence, parameters  $a_1$  and  $a_2$  from Table 1 were calibrated such that the cumulative contribution  $T_2$  accounts for 75-80% of the total dissipation after 12 hours of simulation.

The calibration procedure carried out by Rogers et al. (submitted) that yields to the four dissipation models listed in Table 1 matched the total energy in academic duration-limited simulations to pre-existing physics in the 3G wave model SWAN which however did not consider any other metric associated with the spectral distribution of energy.

### 3 Simulations

In order to evaluate the performance of the observation-based input and dissipation in WAVEWATCH III<sup>TM</sup> (labeled STX hereafter), simulations for wind-dominated conditions of low to medium range wind forcing were carried out for each of the four dissipation models listed in Table 1. The evolution covers an idealised duration-limited academic test and comparisons of integral metrics between NODC<sup>3</sup> buoys and Lake Michigan hindcast.

#### 3.1 Academic test

The academic test is an idealised duration-limited simulation of the wave evolution for a single point in the infinite ocean and under homogeneous wind-forcing with a wind speed of  $12 \text{ m s}^{-1}$  and constant wind direction commencing from calm conditions. Wind-wave evolution for new wind-input and breaking functions was investigated by two means of nonlinear interactions: with DIA (discrete interactive approximation, Hasselmann et al., 1985) parameterisation and with exact computations (XNL for exact nonlinear hereafter) by means of WRT<sup>4</sup> (Tracy and Resio, 1982). The latter

provides accurate estimates of energy fluxes within the wave system, in addition to those due to wind and breaking, but is computational expensive. The former is a fast approximate and thus routinely employed in operational forecast. The duration of this test is limited to 12 hours of simulation with a global time stepping of 30 seconds (15 seconds for source term integration). Spectral properties feature 24 directions and 40 frequencies, logarithmically spaced between  $f = 0.042 \dots 1.7 \text{ Hz}$ . The performance of the academic test is compared against existing physics: TC96 (Tolman and Chalikov, 1996), WAM3 (Komen et al., 1984), and WAM4 (Ardhuin et al., 2010).

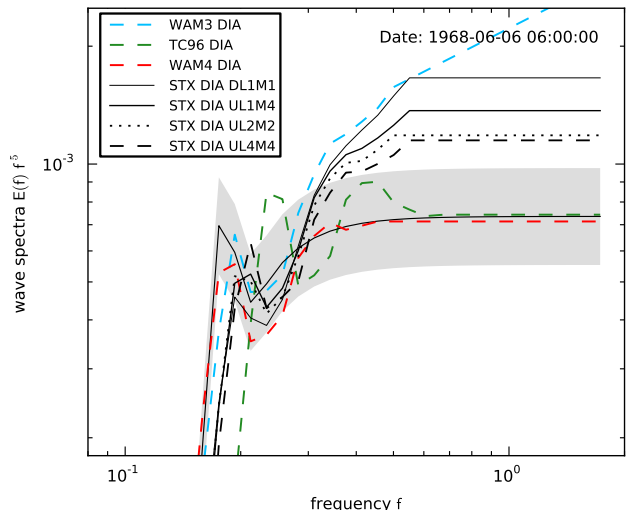


Fig. 4: Level of the spectral tail versus frequency after 6 hours of simulation. Shaded areas represent the observational parameterisation of Babanin and Soloviev (1998a) with 95% confidence limits.

<sup>3</sup> U.S. National Oceanographic Data Center, available online: <http://www.nodc.noaa.gov/BUOY/>  
<sup>4</sup> Webb-Resio-Tracy method

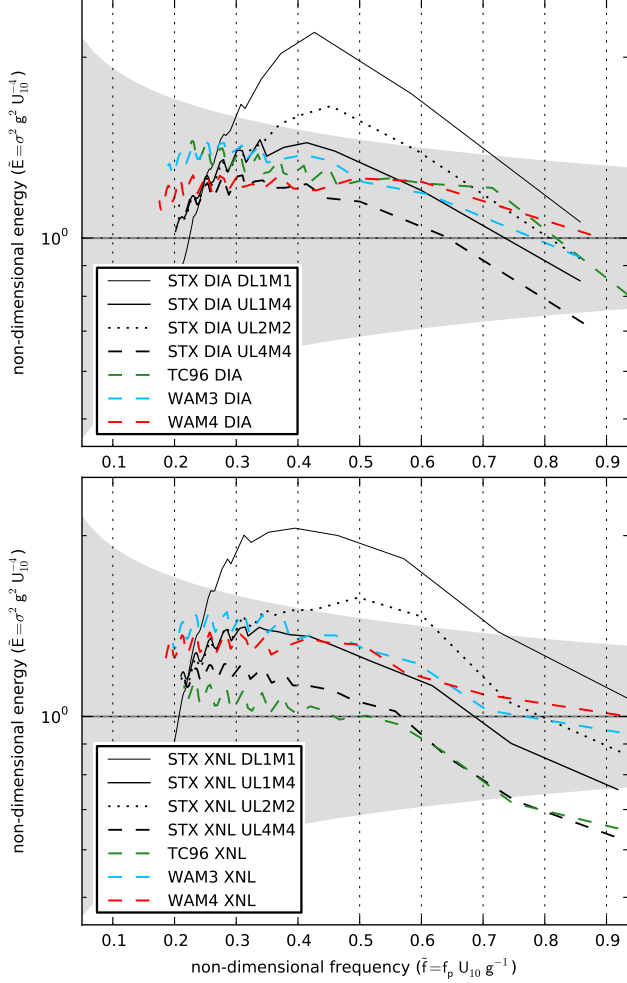


Fig. 5: Non-dimensional wave evolution by means of total wave energy versus peak frequency for selected source functions with (top) DIA and (bottom) XNL. The dependences are normalised by the observational parameterisation of Babanin and Soloviev (1998a) with shaded areas showing 95% confidence limits.

Integral growth curves shown in Figure 5 are usually subject to main scrutiny and tuning and all the source functions perform reasonably well with respect to the experimental dependence. In Figure 5, results are shown for (top) approximate nonlinear interactions and (bottom) exact nonlinear interactions. Since tuning is typically done with the use of DIA in evolution test, it is noticeable that the performance actually deteriorates once the exact nonlinear term is employed. When normalised by the observational parameterisation of Babanin and Soloviev (1998a) with respect to the 95% confidence intervals (shaded gray), the non-dimensional evolution of dissipation models UL1M4 and UL4M4 are in good agreement to the existing physics TC96, WAM3 and WAM4.

For the level of the spectral tail, all four new dissipation parameterisations overestimate the tail in a similar fashion to WAM3 as illustrated in

Figure 4 which shows the spectrum after 6 hours of simulation by means of approximate nonlinear interaction computation (DIA). Figure 4 also shows the observational parameterisation of Babanin and Soloviev (1998a) with 95% confidence limits in respect to the peak frequency  $f_p^{\text{WAM4}} = 0.175$  Hz as estimated by WAM4 simulation. Estimates of peak frequency for all other source terms are:  $f_p^{\text{WAM3}} = 0.187$  Hz,  $f_p^{\text{TC96}} = 0.232$  Hz, and  $f_p^{\text{STX}} \approx 0.19$  Hz, for WAM3, TC96, and the observation-based physics, respectively. Of all four dissipation models, parameterisation UL4M4 features the lowest level of the spectral tail, however, still significantly exceeding observed levels and levels of TC96 and WAM4. As the waves develop the level of the spectral tail increases (not shown). Due to the high level of the spectral tail metrics of higher moments in the hindcast of Lake Michigan are expectedly biased (see later section 3.2).

Figure 6 compares the ratios of existing physics relative to the observation-based parameterisation UL4M4 ( $U_{10}/c_p = 1.5$ ) after 6 hours of simulation (legend and time as in Fig. 4). When compared to the observation-based parameterisation of Donelan et al. (2006), WAM3 and WAM4 wind input is consistently overestimating up to a factor of 10 between 1.0 and 2.0 peak frequencies. In contrast, differences to TC96 wind input are from overestimating to underestimating by a factor of 5. This higher wind input is essentially compensated by the dissipation of similar magnitude, except for TC96 dissipation where between 1.4 and 2.0 peak frequencies the dissipation is underestimating by a factor of 2 (Fig. 6, bottom subplot).

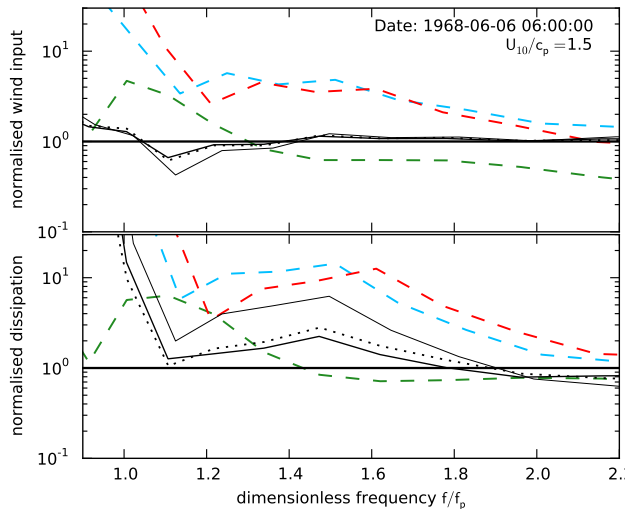


Fig. 6: (Top) wind input and (bottom) dissipation after 6 hours as a function of relative peak frequency normalised by observation-based model UL4M4 (legend as in Fig. 4).

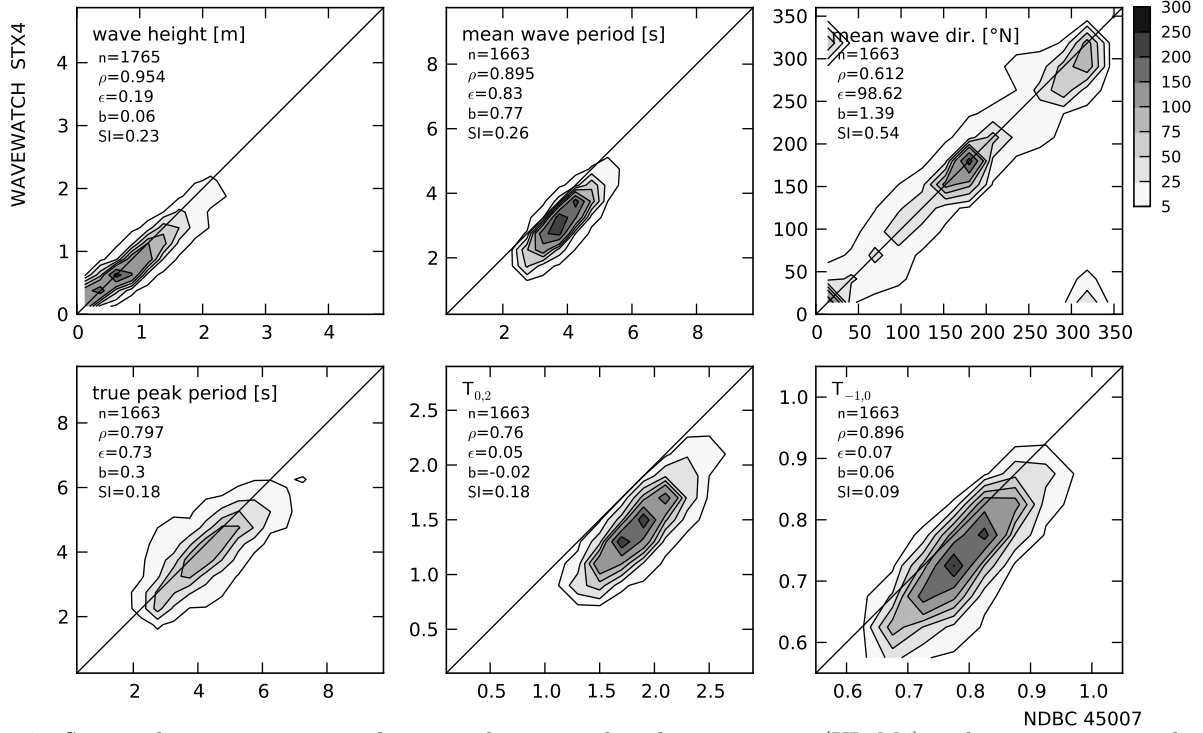


Fig. 7: Scatter density comparisons between observation-based source terms (UL4M4) with approximate nonlinear interactions (DIA) and NODC buoy 45007 located  $42.67^\circ$  N and  $87.02^\circ$  W. Each of the legends indicates scatter statistics: number of scatter points, correlation coefficient, root-mean-square error, bias, and scatter index.

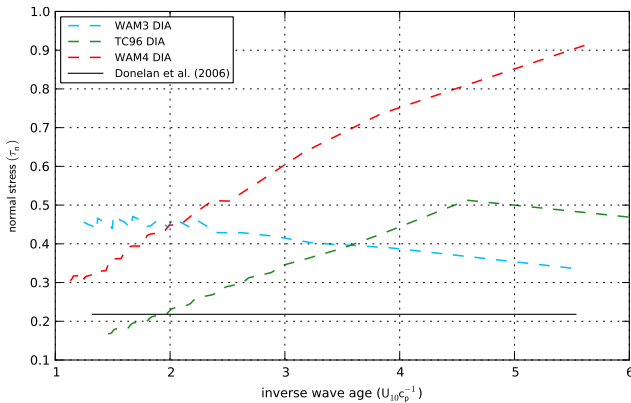


Fig. 8: The normal stress  $\tau_n$  as a function of inverse wave age  $U_{10}/c_p$ . The normal stress was calculated from the wind-input (15).

The apparent overestimate of the wind input shown in Figure 6 is partially due to constraint applied to the wind input, that is the wave induced stress should equal the normal stress exercised by the wind. Figure 8 shows the normal stress  $\tau_n$  as calculated from (15) as a function of inverse wave age  $U_{10}/c_p$  for all existing source functions. At inverse wave age of  $U_{10}/c_p = 1.5$  the normal stress exceeds the wave induced stress by 2.4 times for WAM3 and 1.6 times for WAM4 while it accounts only for 80% for TC96 physics. Note that, none of the existing physics applies a constraint on the normal stress  $\tau_n$ . However, WAM4 computes the value of  $\tau_n$  from the wind-input in order to estimate the friction velocity

$u_*$  ( $\tau = \tau_v + \tau_n = \rho_a u_*^2$ ) and the roughness surface length, where as all other source term packages use various sea-drag parameterisations to estimate drag coefficient  $C_d$  and friction velocity  $u_*$ .

### 3.2 Lake Michigan

The Lake Michigan hindcast is a real test case that simulates windsea-dominated conditions. The generation of swell is essentially prevented due to the limited fetch and the topography of the lake. Lake Michigan is instrumented with two NODC buoys located in the southern and the northern center of the lake respectively. The duration of the hindcast covers a period of 45 days, from 1 September to 14 November 2002, with a time stepping of 7.5 minutes (15 seconds for source term integration). Spectral properties are set to 36 directions and 29 frequencies logarithmically scaled between  $f = 0.07 \dots 0.9$  Hz. At every full hour of the hindcast, the performance of observation-based dissipation model UL4M4 is compared against *in situ* instruments: NODC buoys 45002 and 45007. Note that, only for the latter station directional data is available for the period of the hindcast.

Since, for the new dissipation model UL4M4, the growth curves of total wave energy are reproduced well in the academic test (see Fig. 5), so are the integral wave properties as shown in Figure 6 (i.e. wave height, true peak period, and mean wave direction). However, the overestimate of the

spectral tail yields to an apparent bias in the higher-moment periods: mean wave period ( $T_{01}$ ),  $T_{02}$ , and  $T_{-10}$ . Higher-moment periods depend on the higher-moment spectra in which case the period is proportional to the ratio of two spectral moments following the form:  $T_{ij} \propto m_i/m_j$ , where for  $n = i, j$   $m_n$  is the  $n^{\text{th}}$ -order-moment of the spectrum defined as  $m_n = \int \omega^n F(\omega) d\omega$  (Holthuijsen, 2007).

### 3.3 Calibration and fine tuning

As a result of the academic test and the Lake Michigan hindcast, additional calibration and tuning is required to match the level of the spectral tail and higher-moment periods. It is now known experimentally that at strong forcing at a particular scale the extra wind energy flux cannot be effectively transferred by nonlinear interactions and a part of it is dissipated locally (Babanin and Young, 2005; Babanin et al., 2007b). This effect should reduce the tail level and is now parameterised in order to optimise the tail and higher-moment metrics. This was done by introducing a frequency dependent non-dimensional correction factor  $R$  in a way that the total dissipation (17) corrects to:  $S_{ds} = R S_{ds}$ . In fact, the correction postulated here disproportionately enhances the dissipation at the high-frequency tail of the spectrum to match the observational parameterisation of Babanin and Soloviev (1998a) with 95% confidence limits (as in Fig. 4) with only little impact on the integral growth curves (Fig. 5). The dissipation enhancement factor  $R$  is given in (21).

$$R = \max \left\{ 1, \exp \left( a_3 \exp \left( a_4 \frac{U_{10}}{c_p} \right) \left[ \frac{U_{10}}{c} - a_5 \right] \right) \right\} \quad (21)$$

In (21), coefficients  $a_3$  accommodate for the magnitude of the tail correction while  $a_4$  provides additional control as a function of wave development (i.e. inverse wave age  $U_{10}/c_p$ ). Since the additional control function  $\exp(a_4 U_{10}/c_p)$  grows with wave development, values of coefficient  $a_4$  are negative. Coefficient  $a_5$  serves as a threshold value for which, when exceeded, the tail correction kicks in. For each of the four dissipation models the coefficients  $a_3$ ,  $a_4$ , and  $a_5$  are listed in Table 2, in extension to dissipation models in Table 1.

Tab. 2: The four dissipation models (see Tab. 1) extended by coefficients  $a_3$ ,  $a_4$ , and  $a_5$  for the correction (21) of the level of the high-frequency tail of the spectrum.

	$a_3$	$a_4$	$a_5$
DL1M1	3.8	-0.72	2.4
UL2M2	26.1	-1.93	2.4
UL1M4	27.9	-1.87	2.4
UL4M4	64.1	-2.48	2.4

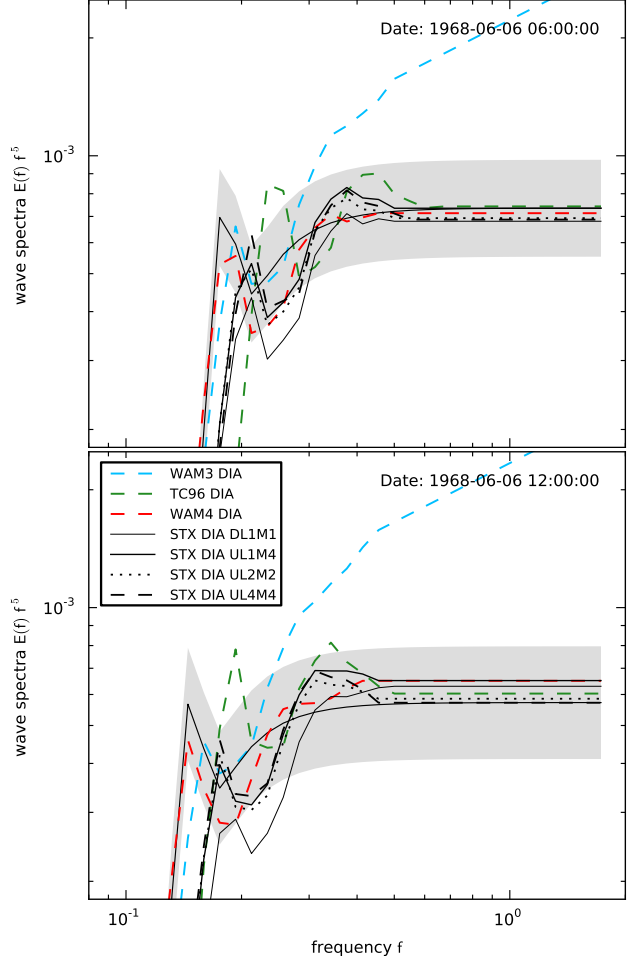


Fig. 9: Level of the spectral tail versus frequency with enhancement factor  $R$  (21) applied after (top) 6 hours and (bottom) 12 hours of simulation. Shaded areas represent the observational parameterisation of Babanin and Soloviev (1998a) with 95% confidence limits.

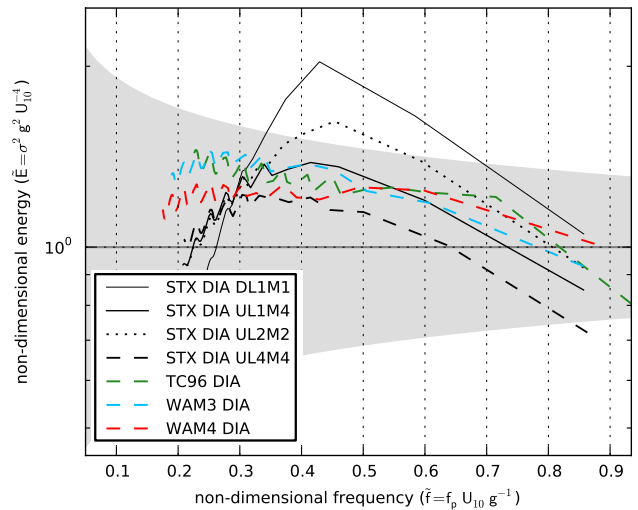


Fig. 10: Non-dimensional wave energy evolution by means of total wave energy versus peak frequency for selected source functions. The dependences are normalised by the observational parameterisation of Babanin and Soloviev (1998a) with shaded areas showing 95% confidence limits.

The performance of the tail correction in the academic test with approximate nonlinear interactions (DIA) is shown in Figure 9 and Figure 10. The latter shows the growth curves of total energy in a similar fashion to those plotted in Figure 5. The former shows the level of the spectral tail which is when compared to Figure 4 now in good agreement with observational parameterisation of Babanin and Soloviev (1998a) for frequencies greater than 0.3 Hz. Results are shown for 6 hours and 12 hours of simulation.

The Lake Michigan hindcast with the tail correction applied yield almost identical scatter density plots (not shown) as in Figure 7. As expected, the higher-moment periods perform slightly better as illustrated in Figure 11, but improvements are marginal. The energy in the high frequency part of the spectrum seem to have little impact on the total wave energy higher-order moments of the spectrum.

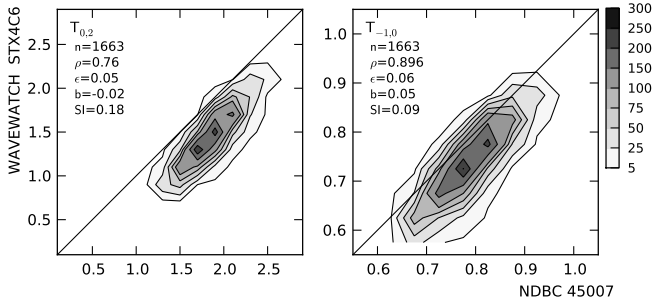


Fig. 11: Scatter density comparison of observation-based source terms (UL4M4) with approximate nonlinear interactions (DIA) in the Lake Michigan hindcast for the same location as in Fig. 7 but with enhancement factor  $R$  (21) applied with only higher-moment periods  $T_{0.2}$  and  $T_{-1.0}$  shown. Other integral parameters performed as well as before and are therefor omitted.

## 4 Summary and future work

The observation-based source terms implemented in WAVEWATCH III<sup>TM</sup> were tested in a duration-limited academic test and the Lake Michigan hindcast. These tests showed that the total energy is in good agreement with observations by means of the parameterisation by Babanin and Soloviev (1998a) (see Fig. 9 and Fig. 10) and buoy data (see Fig. 7). However, scatter comparisons between NODC buoy 45007 and the Lake Michigan hindcast also show that the observation-based source terms underestimate true peak period, mean wave period  $T_{0.1}$  and higher moment periods  $T_{0.2}$  and  $T_{-1.0}$  even with the high level of the spectral tail adjusted (Fig. 9) using the correction factor (21). One possible reason for these results might be the distribution of energy along all discrete directions. For example, the constraint applied on

Tab. 3: Metrics used to assess the performance of the observation-based source terms. Tested metrics are marked with crosses while dashes indicate metrics that still need to be verified unless it is not applicable (i.e. n/a). The metrics tabulated cover: dimensionless energy  $\tilde{E}$ , dimensionless peak frequency  $\tilde{f}_p$ , fetch  $\tilde{x}$ , and time  $\tilde{t}$ , wave height  $H_s$ , wave periods  $T_p$  and  $T_n$ , wave direction  $\theta$ , peak frequency  $f_p$ , the level of the spectral tail  $\alpha$ , spectral peakedness  $\gamma$ , transitional frequency  $\omega_t$ , directional narrowness  $A$ , directional spreading  $D_\theta$ , wave induced stress (as scalar  $\tau_n$  and vector  $\vec{\tau}_n$ ), wind input  $S_{in}$ , wave dissipation  $S_{ds}$ , the ratio of input and dissipation and swell dissipation  $S_{wl}$ .

METRICS	ACADEMIC TEST	HINDCAST	
	duration-limited	Lake Michigan	
growth curves	$\tilde{E}$ vs. $\tilde{f}_p$	x	n/a
	$\tilde{E}$ vs. $\tilde{x}$	n/a	n/a
	$\tilde{E}$ vs. $\tilde{t}$	–	n/a
integral parameters	$H_s$	n/a	x
	$T_p$	n/a	x
	$T_n$	n/a	x
	$\theta$	n/a	x
	$f_p$	n/a	x
spectral parameters	$\alpha$	x	–
	$\gamma$	–	–
	$\omega_t$	–	–
directional parameters	$A(f_p)$	–	–
	$A(2f_p)$	–	–
	$D_\theta$	–	–
constraints	$\tau_n$	x	n/a
	$\vec{\tau}_n$	–	n/a
	$S_{in}$	x	n/a
	$S_{ds}$	x	n/a
	$S_{ds}S_{in}^{-1}$	–	n/a
	$S_{wl}$	–	n/a

the normal stress  $\tau_n$  and the “two-phase” behaviour of the wave-breaking and dissipation term  $T_1$  and  $T_2$  are based on non-directional parameterisations. Therefore, additional testing need to be carried out in order to qualify the directional distribution of energy of the spectrum (see directional metrics listed in Table 3), which also plays a significant role in situations of turning wind fields (i.e. greater than  $90^\circ$ ) and for opposing winds.

At this stage, the implementation of the observation-based source terms lacks swell dissipation  $S_{wl}$  and the white-capping dissipation  $S_{ds}$  remains zero if the spectral energy density does not exceed the threshold spectral density  $F_T$ . Also, in case of opposing wind forcing, the growth rate  $\gamma$  in the wind input parameterisation remains zero, but laboratory experiment conducted by Donelan (1999) showed that the growth rate becomes negative if  $U_{\lambda/2}/c - 1 < 0$ , where  $U_{\lambda/2}$  is the wind speed at a height of one-half the wave length  $\lambda$ . This plays

a significant role in order to model open-ocean conditions and conditions of extreme wind forcing such as hurricanes or tropical cyclones. The swell dissipation will be implemented after Babanin (2011), in which the dissipation is due to turbulent mixing of the water column as a function of the orbital velocity of the waves at the surface, after Ardhuin et al. (2009), in which it is due to interaction with atmospheric turbulence, and after Donelan (1999) in which it is due to waves interacting with opposing winds.

## References

- Ardhuin, F., B. Chapron, and F. Collard, 2009: Observation of swell dissipation across oceans. *Geophys. Res. Lett.*, **36**, L06 607, 5 pp., doi:10.1029/2008GL037030.
- Ardhuin, F., et al., 2010: Semiempirical dissipation source functions for ocean waves. Part I: Definition, calibration, and validation. *J. Phys. Oceanogr.*, **40** (9), 1917–1941, doi:10.1175/2010JPO4324.1.
- Babanin, A., 2011: *Breaking and Dissipation of Ocean Surface Waves*. Cambridge University Press, 485 pp.
- Babanin, A. and V. Makin, 2008: Effects of wind trend and gustiness on the sea drag: Lake george study. *J. Geophys. Res.*, **113**, C02015, 18pp., doi:10.1029/2007JC004233.
- Babanin, A. V., 2009: Breaking of ocean surface waves. *Acta Phys. Slovaca*, **59**, 305–535.
- Babanin, A. V., M. L. Banner, and I. R. Young, 2001: Breaking probabilities for dominant surface waves on water of finite constant depth. *J. Geophys. Res.*, **106** (6), 11,659–11,676, doi:10.1029/2000JC000215.
- Babanin, A. V., M. L. Banner, I. R. Young, and M. A. Donelan, 2007a: Wave-follower field measurements of the wind-input spectral function. Part III: Parameterization of the wind-input enhancement due to wave breaking. *J. Phys. Oceanogr.*, **37** (11), 2764–2775, doi:10.1175/2007JPO3757.1.
- Babanin, A. V. and Y. P. Soloviev, 1998a: Field investigation of transformation of the wind wave frequency spectrum with fetch and the stage of development. *J. Phys. Oceanogr.*, **28** (4), 563–576, doi:10.1175/1520-0485(1998)028<0563:FIOTOT>2.0.CO;2.
- Babanin, A. V. and Y. P. Soloviev, 1998b: Variability of directional spectra of wind-generated waves, studied by means of wave staff arrays. *Mar. Freshwater Res.*, **49** (2), 89–101, doi:10.1071/MF96126.
- Babanin, A. V., K. N. Tsagareli, I. R. Young, and D. J. D. Walker, 2007b: Implementation of new experimental input/dissipation terms for modeling spectral evolution of wind waves. *Proc. 10th Int. Workshop on Wave Hindcasting and Forecasting*, Oahu, HI, 11-16 November, 12pp.
- Babanin, A. V., K. N. Tsagareli, I. R. Young, and D. J. Walker, 2010: Numerical investigation of spectral evolution of wind waves. Part II: Dissipation term and evolution tests. *J. Phys. Oceanogr.*, **40** (4), 667–683, doi:10.1175/2009JPO4370.1.
- Babanin, A. V. and A. J. v. Westhuysen, 2008: Physics of “saturation-based” dissipation functions proposed for wave forecast models. *J. Phys. Oceanogr.*, **38** (8), 1831–1841, doi:10.1175/2007JPO3874.1.
- Babanin, A. V. and I. R. Young, 2005: Two-phase behaviour of the spectral dissipation of wind waves. *Proc. Fifth Int. Symp. Ocean Waves Measurement and Analysis*, Madrid, Spain, 3-7 July, 11pp.
- Banner, M., A. V. Babanin, and I. R. Young, 2000: Breaking probability for dominant waves on the sea surface. *J. Phys. Oceanogr.*, **30** (12), 3145–3160, doi:10.1175/1520-0485(2000)030<3145:BPFOW>2.0.CO;2.
- Banner, M. L., J. R. Gemmrich, and D. M. Farmer, 2002: Multiscale measurements of ocean wave breaking probability. *J. Phys. Oceanogr.*, **32**, 3364–3375, doi:10.1175/1520-0485(2002)032<3364:MMOOWB>2.0.CO;2.
- Banner, M. L. and W. L. Peirson, 1998: Tangential stress beneath wind-driven air–water interfaces. *J. Fluid. Mech.*, **364**, 115–145, doi:10.1017/S0022112098001128.
- Booij, N., R. C. Ris, and L. H. Holthuijsen, 1999: A third-generation wave model for coastal regions I. model description and validation. *J. Geophys. Res.*, **104** (4), 7649–7666, doi:10.1029/98JC02622.
- Donelan, M., 1999: Wind-induced growth and attenuation of laboratory waves. *Wind-over-wave couplings: perspectives and prospects*, S. G. Sajadi, N. H. Thomas, and J. C. R. Hunt, Eds., Clarendon Press, 183–194.
- Donelan, M. A., A. V. Babanin, I. R. Young, and M. L. Banner, 2006: Wave-follower field measurements of the wind-input spectral function. Part II: Parameterization of the wind input. *J. Phys. Oceanogr.*, **36** (8), 1672–1689, doi:10.1175/JPO2933.1.
- Donelan, M. A., A. V. Babanin, I. R. Young, M. L. Banner, and C. McCormick, 2005: Wave-follower field measurements of the wind-input spectral function. Part I: Measurements and calibrations. *J. Atmos. Ocean. Tech.*, **22** (7), 1672–1689, doi:10.1175/JTECH1725.1.
- Hasselmann, K., R. K. Raney, W. J. Plant, W. Alpers, R. A. Shuchman, D. R. Lyzenga, C. L. Rufenach, and M. J. Tucker, 1985: Theory of synthetic aperture radar ocean imaging: A MARSEN view. *J. Geophys. Res.*, **90** (3), 4659–4686, doi:10.1029/JC090iC03p04659.
- Holthuijsen, L. H., 2007: *Waves in Oceanic and Coastal Waters*. Cambridge University Press, 387 pp.
- Hwang, P. A., 2010: A note on the ocean surface roughness spectrum. *J. Atmos. Ocean. Tech.*, **28** (3), 436–443, doi:10.1175/2010JTECHO812.1.
- Komen, G. J., L. Cavaleri, M. Donelan, K. Hasselmann, and P. Janssen, 1994: *Dynamics and Modelling of Ocean Waves*. Cambridge University Press, 532 pp.
- Komen, G. J., S. Hasselmann, and K. Hasselmann, 1984: On the existence of a fully developed wind-sea spectrum. *J. Phys. Oceanogr.*, **14** (8), 1271–1285, doi:10.1175/1520-0485(1984)014<1271:OTEOAF>2.0.CO;2.
- Longuet-Higgins, M. S. and R. W. Stewart, 1961: The changes in amplitude of short gravity waves on steady non-uniform currents. *J. Fluid. Mech.*, **10** (4), 529–549, doi:10.1017/S0022112061000342.
- Phillips, O. M., 1961: On the dynamics of unsteady gravity waves of finite amplitude Part 2. local properties of a random wave field. *J. Fluid. Mech.*, **11** (1), 143–155, doi:10.1017/S0022112061000913.

- Phillips, O. M., 1984: On the response of short ocean wave components at a fixed wavenumber to ocean current variations. *J. Phys. Oceanogr.*, **14** (9), 1425–1433, doi:10.1175/1520-0485(1984)014<1425:OTROSO>2.0.CO;2.
- Pierson, W. J. and L. Moskowitz, 1964: A proposed spectral form for fully developed wind seas based on the similarity theory of S. A. Kitaigorodskii. *J. Geophys. Res.*, **69** (24), 5181–5190, doi:10.1029/JZ069i024p05181.
- Reul, N., H. Branger, and J.-P. Giobanangeli, 1999: Air flow separation over unsteady breaking waves. *Phys. Fluid.*, **11** (7), 1959–1961, doi:10.1063/1.870058.
- Rogers, W. E., A. V. Babanin, and D. W. Wang, submitted: Observation-based input and whitecapping-dissipation in a model for wind-generated surface waves: Description and simple calculations. *J. Phys. Oceanogr.*
- Tolman, H. L., 2009: User manual and system documentation of WAVEWATCH III™ version 3.14. Tech. note 276, Enviro. Modelling Center, 220 pp., Camp Springs, MD.
- Tolman, H. L. and D. Chalikov, 1996: Source terms in a third-generation wind wave model. *J. Phys. Oceanogr.*, **26** (11), 2497–2518, doi:10.1175/1520-0485(1996)026<2497:STIATG>2.0.CO;2.
- Tracy, B. and D. T. Resio, 1982: Theory and calculations of the nonlinear energy transfer between sea waves in deep water. WES Rep. 11, US Army Corps of Engineers, 54 pp.
- Tsagareli, K. N., A. V. Babanin, D. J. Walker, and I. R. Young, 2010: Numerical investigation of spectral evolution of wind waves. Part I: Wind-input source function. *J. Phys. Oceanogr.*, **40** (4), 656–666, doi:10.1175/2009JPO4345.1.
- van Vledder, G. P., 2002: Improved parameterisations of nonlinear four-wave interactions for applications in operational wave prediction models. Alkyon rep. 151, 55 pp.
- Young, I. R., 1999: *Wind Generated Ocean Waves*. Elsevier Ocean Engineering Series, Elsevier Science, 306 pp., doi:10.1016/S0378-3839(00)00061-2.
- Young, I. R. and A. V. Babanin, 2006: Spectral distribution of energy dissipation of wind-generated waves due to dominant wave breaking. *J. Phys. Oceanogr.*, **36** (3), 379–394, doi:10.1175/JPO2859.1.